Hydrogel-Based Tunable-Focus Liquid Microlens Array With Fast Response Time

Difeng Zhu, Chi-Wei Lo, Chenhui Li, and Hongrui Jiang, *Senior Member, IEEE*

***Abstract*—We present a hydrogel-driven focus-tunable liquid microlens array on a curvilinear surface with much faster response time than previously reported. Water–oil interfaces pinned at polymer apertures serve as microlenses. Thermoresponsive poly(*N*-isopropylacrylamide) hydrogel incorporating glycidyl-methacrylate-functionalized graphene oxide is employed to provide faster actuation for focal length tuning. Thermoelectric modules based on Peltier effect were implemented to enhance the heat transfer to and dissipation from the hydrogel actuators. The average response time improves to 5 s, and the focal length ranges from 7 to 120 mm. Simulations were performed to characterize the thermal behavior of the microlens array during actuation. The microlens array is also demonstrated with an ability to be remotely controlled by infrared light. [2011-0285]**

***Index Terms*—Curvilinear surface, microlens array, response time, thermal analysis, tunable focus.**

I. Introduction

As AN indispensable component in imaging and microscopy, microlens plays an important role in biomedical, industrial, and military applications [1]–[6]. Furthermore, microlenses and microlens arrays with more functionalities such as focus tunability, large field of view (FOV), and structural robustness are highly desired [1], [3], [6]–[8]. Compared to tunable microlenses based on other mechanisms such as liquid crystal [3], electrowetting [9], fluidic pressure [10], and electrochemical reaction [2], hydrogel microlenses and microlens arrays have shown great promise, since they offer large tuning range, good biological compatibility, and relative convenience to integrate with optics. Moreover, the hydrogel-driven microlens array could be fabricated onto nonplanar surfaces with large FOV, which could have greater scope of applications [7], [12]–[14]. Nevertheless, relatively slow response time on the order of tens of seconds could limit their potential applications.

Here, we present a thermoresponsive-hydrogel-actuated microlens array on a hemispheric dome with much faster response time than previously reported. The improvement is attributed to two factors. First, glycidyl methacrylate (GMA)-functionalized graphene oxide (GO) was incorporated into the thermoresponsive poly(*N*-isopropylacrylamide) (PNIPAAm) hydrogel [15] (called GO-GMA hydrogel). This GO-GMA hydrogel has much faster thermal response compared to the original PNIPAAm hydrogel and is employed to provide more effective actuation for focal length tuning. Second, the delivery and dissipation of heat to the hydrogel actuators are much enhanced. The slow response time of the previously reported hydrogel-driven liquid microlenses [7], [12], [13] is mainly due to the reliance on the natural heat dissipation through the structures when the hydrogel needs to be cooled down. We applied thermoelectric modules based on the Peltier effect and assembled them close to the hydrogel actuators to facilitate the local cooling process. These modules also improved the local heating process of the hydrogel. The microlens array was fabricated on a curvilinear surface (a hemispherical shell) to achieve large FOV, utilizing a relatively simple process.

Simulations and experiments on the thermal stress and crosstalk between adjacent microlenses during the actuation processes were performed in order to further characterize the tuning behavior of the microlens array. It was demonstrated that the operation of the microlens array was not affected by the thermal disturbance such as thermal stress and crosstalk during the actuation.

Owing to the strong infrared (IR) light absorption in GO within the hydrogel networks and the photothermal energy conversion capability of GO to trigger the hydration–dehydration transition, the GO-GMA-hydrogel-based microlens array can also be remotely controlled by IR irradiation, which could have more potential applications [15], [16]. Characterization of the IR-responsive microlens array is also discussed.

II. Principle and Structure

Fig. 1(a) and (b) shows the 3-D schematics of one GO-GMA-hydrogel-driven liquid microlens in an array fabricated on a hemispherical shell. A cavity, defined by a polydimethylsiloxane (PDMS) polymer substrate and a PDMS aperture slip, is filled with water. Silicone oil is added on top of the water to prevent evaporation and serve as the lens material due to its higher refractive index (1.48) compared to that of water (1.33). The sidewall of the aperture slip is treated hydrophilic, while

Manuscript received September 23, 2011; revised March 30, 2012; accepted April 7, 2012. Date of publication May 11, 2012; date of current version September 27, 2012. This work was supported mainly by the National Science Foundation under Grant ECCS 0745000 and partly by the Wisconsin Institutes for Discovery and the Wallace H. Coulter Foundation. Subject Editor O. Solgaard.

D. Zhu was with the Department of Electrical and Computer Engineering, University of Wisconsin, Madison, WI 53706 USA. He is now with Micron Technology, Inc., Boise, ID 83705 USA (e-mail: difengzhu@micron.com).

C.-W. Lo was with the Materials Science Program, University of Wisconsin, Madison, WI 53706 USA. He is now with Applied Materials Inc., Santa Clara, CA 95054 USA (e-mail: clo3@wisc.edu).

C. Li is with the Department of Electrical and Computer Engineering, University of Wisconsin, Madison, WI 53706 USA (e-mail: cli26@wisc.edu).

H. Jiang is with the Department of Electrical and Computer Engineering, the Materials Science Program, the Eye Research Institute, and the Department of Biomedical Engineering, University of Wisconsin, Madison, WI 53706 USA (e-mail: hongrui@engr.wisc.edu).

Color versions of one or more of the figures in this paper are available online at http://ieeexplore.ieee.org.

Digital Object Identifier 10.1109/JMEMS.2012.2196492

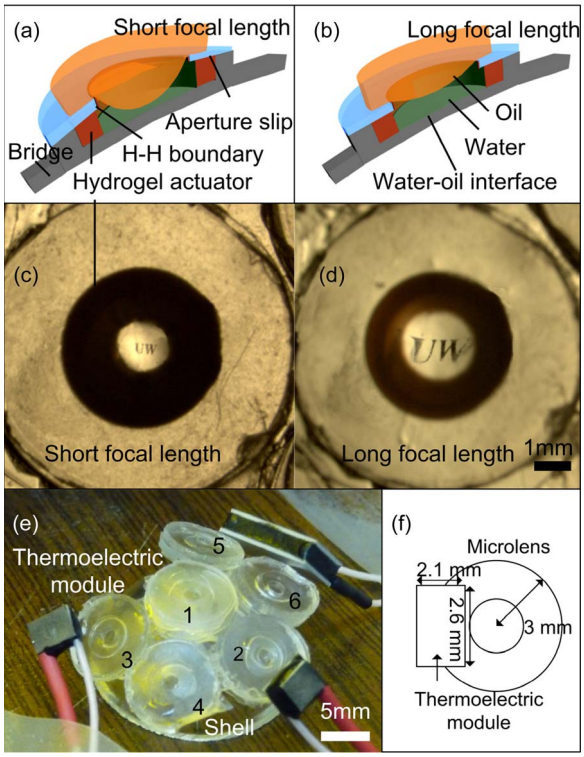

Fig. 1. (a) and (b) Schematics of one microlens with short and long focal lengths, respectively. A PDMS aperture slip and an underlying PDMS substrate form a cavity. GO-GMA hydrogel is patterned in the cavity as the actuator. The sidewalls of the aperture are chemically treated hydrophilic, while the top surfaces are naturally hydrophobic. A curved water-oil interface pinned by the H-H boundary forms a liquid-based microlens. Contracted hydrogel corresponds to longer focal length with less curved meniscus; expanded hydrogel brings about shorter focal length with more curved meniscus. (c) and (d) Optical images of a microlens with a shorter and a longer focal length, respectively. The left image (shorter focal length) was taken at around 30 °C; the right image (long focal length) was taken at about 50 °C. The scale bar represents 1 mm. (e) Image of a six-element microlens array on a shell with a diameter of 18 mm. The thermoelectric modules assembled around the lenses regulate the temperature of the microlenses. Each microlens is labeled with a number. The scale bar is 5 mm. (f) Schematic of thermoelectric module position on the microlens.

the top surface of the PDMS slip is naturally hydrophobic [7], [8], [12]. Thus, a water–oil meniscus, whose circumference is pinned by a hydrophobic–hydrophilic (H-H) boundary at the top edge of the aperture, functions as a microlens. Several GO-GMA-hydrogel sectors are photopatterned in the cavity, acting as the actuators to tune the focal length of the microlenses. As the temperature decreases, the hydrogel expands in vertical direction and tilts the aperture slip toward the oil, which, in turn, pushes the edge pinning the water-oil meniscus more into the oil. Thus, with the presence of the oil pressure and the surface tension, the water in the cavity tends to be squeezed away from the central area and accumulates at the peripheral area close to the polymer slip. As a result, at the center, the oil protrudes more into the water, creating an oil–water interface with smaller radius of curvature, as shown in Fig. 1(a), thus shortening the focal length. While the temperature increases, the hydrogel shrinks, and the aperture slip tilts toward the water, which would, in turn, exert pressure onto the water in the cavity at the periphery area. Thus, the water tends to accumulate at the central area, which would push the water-oil interface more into the oil, resulting in a larger radius of curvature, which means an increase in focal length, as shown in Fig. 1(b). To provide local heating and cooling of the hydrogel actuators, several thermoelectric modules (TE-8-0.45-1.3 and TE-35-0.6-1, TE Technology, Inc., Traverse City, MI) are assembled around the microlenses. Fig. 1(c) and (d) shows the optical images of a microlens in two states, respectively. A smaller image in the liquid microlens indicates a shorter focal length of the microlens, and a larger image indicates a state with a longer focal length. The complete six-element microlens array fabricated on a hemispherical shell with thermoelectric modules is shown in Fig. 1(e). Thermoelectric modules are placed on the outer area of the aperture slips of the microlenses, as shown in Fig. 1(f).

III. Materials and Fabrication

The fabrication process is based on a soft lithography process [7], [8], [17] without clean room environment. Five masked ultraviolet (UV) exposures were performed to form the microlens structure. The geometry of the structure of the microlens array and the connection bridges between the lens elements was defined by the first two UV exposures, while the third and fourth UV exposures determined the geometry of the aperture slip and barriers. A polymer microlens array structure was realized by pattern replica molding. The last UV exposure was utilized to define the shape of the thermoresponsive hydrogels as actuators.

Photopolymerization procedures in the fabrication were carried out using a desktop EXFO Acticure 4000 (EXFO Photonic Solutions, Inc., Missisauge, ON, Canada) UV light source. Photomasks were printed on high-resolution films (3000 dpi, Imagesetter, Inc., Madison, WI, USA). Oxygen plasma treatments were carried out using corona plasma discharge.

A. Materials

There were three kinds of polymers used in this fabrication procedure: photopolymerizable prepolymer mixture solution [isobornylacrylate (IBA)] [12], PDMS [17], and GO-GMA hydrogel [15]. IBA acts as molds and functions similar to negative photoresists. With exposure to a UV light source, IBA cross-links, and the prepolymer mixture solution is solidified (called poly-IBA). PDMS performs as the structural polymer of the microlens array, which forms the substrates, the connection bridges, and the apertures based on the IBA molds. PDMS could be cured from its original mixture state at high temperature. The GO-GMA hydrogels, serving as actuators, are responsible for the focus tuning of each microlens. Similar to the original PNIPAAm hydrogel, the GO-GMA hydrogel is thermoresponsive and can be cross-linked under UV radiance in air, like negative photoresists.

The application of GO-GMA hydrogel is essential to realize fast response of the microlenses. With its high efficiency in thermal absorption and conduction [15], [18], the GO incorporated in the PNIPAAm hydrogel significantly enhances the hydration-dehydration transition, thus increasing the tuning speed. A comparison between the GO-GMA hydrogel and the PNIPAAm hydrogel under thermal variance is shown in Fig. 2. Fig. 2(a) shows a GO-GMA-hydrogel film and a PNIPAAm-hydrogel

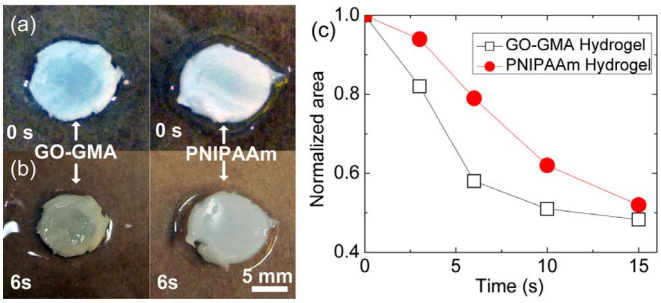

Fig. 2. Comparison of the changes in volume between GO-GMA hydrogel and PNIPAAm hydrogel under thermal variance. (a) GO-GMA- and PNIPAAm-hydrogel films initially in a water-based aqueous environment. (b) GO-GMA- and PNIPAAm-hydrogel films after being heated at 65 °C for 6 s. The scale bar represents 5 mm. (c) Dynamic change in the normalized areas of the films with time.

film with the same initial diameter of 10 mm; both were immersed in water. Then, after being heated at 65 °C on a hot plate for 6 s, the statuses of the hydrogel films are shown in Fig. 2(b). A much more distinct change in area of the GO-GMA-hydrogel film was observed as compared to the PNIPAAm-hydrogel film. The dynamic change in the normalized areas of both films is plotted in Fig. 2(c). Heating at 65 °C started at 0 s. The GO-GMA hydrogel contracted much faster than PNIPAAm, and the shrinkage in area reaches the maximum at around 5 s. As indicated in this experiment, microlens with GO-GMA-hydrogel actuators would have faster tuning speed than that with PNIPAAm hydrogel. The functionality of GO-GMA was tested multiple times, and no apparent hysteresis was observed.

B. Fabrication Process

The fabrication process of the GO-GMA-hydrogel-driven microlens array is shown in Fig. 3, leveraging the method that we previously reported in [8]. First, the IBA substrate mold was formed in a polycarbonate cartridge well (40 mm × 22 mm, HybriWells, Grace Bio-Labs, Inc., Bend, OR, USA). Spacers that are 250 μm thick (double-sided adhesive tape; 3 M Corporate, St. Paul, MN) were placed in the cartridge. An IBA-based prepolymer mixture solution was flowed into the well and was exposed to UV light ($intensity\ of\ UV = 9$ mW/cm^2; time $t =$ 20 s) with Mask I to form a poly-IBA array of wells, as shown in Fig. 3(a) (top view shown on the right). During the exposure, the mask is pushed against the top surface of the cartridge well; therefore, the height of the patterned IBA was defined by the thickness of the spacers. The bottom liner plate of the cartridge was then peeled off. Unpolymerized prepolymer solution was rinsed away with ethanol. Another layer of IBA polymer was subsequently formed onto the patterned structures under UV radiance (intensity $I = 9$ mW/cm^2; time $t = 20$ s) with Mask II to increase the height of selected patterns with 200-μm-thick spacers, corresponding to the ultimate connection bridge structures, as shown in Fig. 3(b). Mask II was aligned on top of the second cartridge with the patterned IBA molding structures utilizing three small circles at the edge, as shown in the right picture (top view) of Fig. 3(b). A similar procedure was executed on a glass slide to form another mold of 120 μm in thickness, corresponding to the aperture slip, as shown in Fig. 3(d). An extra poly-IBA layer with a height of around 200 μm was photopatterned on the original aperture slip pattern with Mask IV, as shown in Fig. 3(e). This layer served as the mold for PDMS barriers, which would prevent oil leakage from the completed device. Both IBA patterns were transferred to PDMS layers functioning as the substrate and the aperture slip, respectively, as shown in Fig. 3(c) and (e). The liquid level of the PDMS mixture was lower than the IBA mold to form through-holes as the apertures. The PDMS mixture was then cured on a hot plate at 65 °C for 4 h. Next, two fully cured PDMS layers were peeled off from their respective molds.

After the inner surfaces of the cavities were treated from hydrophobic to hydrophilic by corona plasma discharge, two PDMS layers were bonded together [19], as shown in Fig. 3(f), to form the structure. Then, the bonded PDMS structure was pressed by 20 lb of loads for one day, in order to prevent leakage between the bonded layers.

Next, a GO-GMA-hydrogel precursor was injected into the cavities, as shown in Fig. 3(g), and was photopatterned under UV light with Mask V, as shown in Fig. 3(h). Three lines across the circle in the mask would divide the GO-GMA hydrogel into six sectors in the cavity. In this way, surfaces of the hydrogel actuators were increased, which exhibited less resistance and more freedom in actuation procedure. As a result, the actuation force and speed provided by the hydrogel were improved, and thus, the response time was decreased correspondingly [20]. The intensity used in lithography was 28 mW/cm^2, which is about twice of that used on PNIPAAm-hydrogel patterns. The exposure time was extended to 25 s to ensure full cross-linking of the GO-GMA hydrogel. Non-cross-linked hydrogel precursor was flushed away by ethanol.

After six sectors of GO-GMA hydrogel were formed in the cavities after the fifth UV exposure, the sidewall of the aperture slip was treated by corona plasma discharge to be hydrophilic to pin the water-oil menisci, as shown in Fig. 3(i).

Then, the planar microlens array with a soft PDMS substrate was wrapped onto a hemisphere base. Finally, each cavity was filled with water and covered by silicone oil, forming the water-oil interfaces, as shown in Fig. 3(j). The diameter of each microlens was 1.8 mm. Each cavity was 250 μm in depth and 4 mm in diameter. The connection bridges were around 200 μm thick, 0.8 mm wide, and 0.8 mm long. These connection bridges, which are much thinner than the lens structure, would effectively absorb the stress owing to the wrapping [8]. θ, defined as the angle that the lens array structure subtends in Fig. 3(j), was 118 °C, hence large FOV as compared to a planar lens array. The shape of the original water-oil interfaces was determined by the volume of water filled.

IV. Optical Characterization

Back focal length measurements and imaging characterization of the GO-GMA-hydrogel-driven liquid microlenses were then performed. First, the microlens under test was set at the shortest focal length (0 s). Then, a thermoelectric module was positioned near the microlens [Fig. 1(f)], operating as a heater to contract the hydrogel for 5 s (forward cycle). Subsequently (at 5 s), the thermoelectric module was reverse connected to

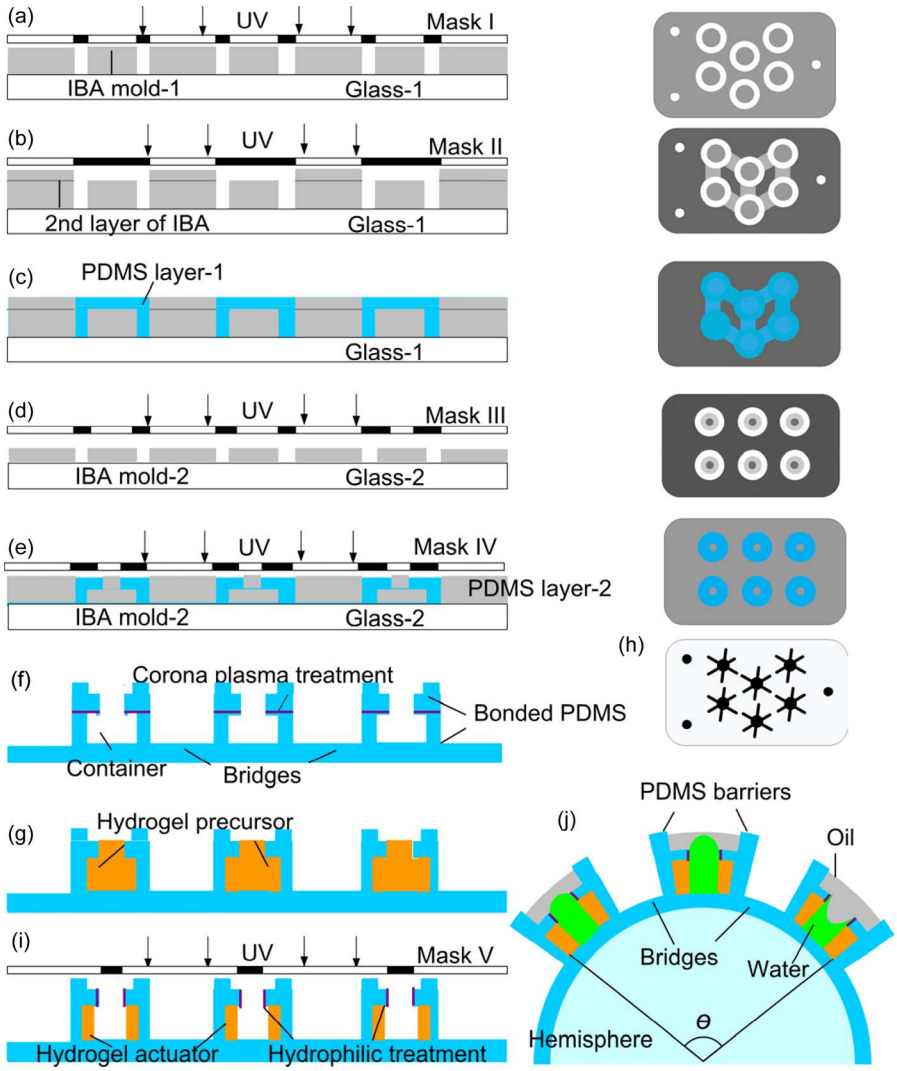

Fig. 3. Fabrication process flow of a six-element tunable-focus microlens array on a hemisphere. (a) IBA layer is initially photopatterned on a glass slide with Mask I. The right picture is the top view of the first layer of IBA mold. (b) Another IBA layer is photopatterned on the original IBA mold with Mask II. Mask II is aligned with the IBA substrate by three small circles on the edge, which could be seen from the top view on the right. By heightening certain parts of the IBA layer in the second lithography step, molds for the connection bridges are realized. (c) PDMS mixture is poured onto the heightened IBA layer. These PDMS patterns serve as the substrates and the connection bridges. The top view of the geometry of the PDMS pattern is shown in the right picture. (d) Another IBA mold is photopatterned on the second glass slide with Mask III. (e) Extra IBA mold is photopatterned with Mask IV serving as the mold for later PDMS barriers. PDMS mixture is partially filled in the IBA mold and cured, serving as the aperture layer of the microlens structure. (f) After being fully cured on hot plates, two PDMS layers are stripped from their molds. Corona plasma treatment is performed on their surface. The microlens cavities are formed by bonding together these two PDMS layers whose surfaces have been treated hydrophilic by corona plasma. The bonding is performed for each individual cavity. (g) GO-GMA-hydrogel precursor is injected into six cavities. (h) Mask V is used to photopattern GO-GMA-hydrogel sectors in the PDMS cavities. (i) GO-GMA-hydrogel sectors are photopatterned in the cavities as actuators, again with Mask V. The sidewall of the aperture slip is treated from hydrophobic to hydrophilic. (j) Water-oil menisci are formed due to surface tension. These water-oil interfaces are formed at the edge of each aperture slip, serving as the lenses. The microlens array is wrapped onto a hemispherical base, distributed on a cap. θ is defined as the angle that this cap subtends.

function as a cooler to expand the hydrogel actuator (reverse cycle). The back focal length of the microlens gradually decreased until 11 s.

The back focal length of each microlens in the array was measured in one complete scanning cycle (forward and reverse) and is plotted in Fig. 4(a). They varied from several millimeters to more than 100 mm. Nonuniformity, as well as nonuniformity in our exposure system for fabrication, stems from different volumes of water initially added into the individual cavity. The setup to test the imaging of the GO-GMA-hydrogel-driven tunable-focus microlens array on the shell is shown in Fig. 4(b). An object plane with logos of "W" (1 mm in size) was positioned 25 mm below this microlens array (including the underlying hemispherical shell). A charge-coupled-device-coupled stereoscope was positioned above this microlens array to monitor and capture images obtained from the microlenses. The frame sequence from the recorded video of one typical microlens (number 2) in one scanning cycle is shown in Fig. 4(c). The images were magnified before 5 s when the thermoelectric module functioned as a heater, indicating an increase in focal length; the image scaled back after 5 s when the thermoelectric module functioned as a cooler, indicating a decrease in focal length. An image of the U.S. Air Force (USAF) 1951 resolution test chart obtained by one liquid microlens in the array is shown in Fig. 4(d), which indicates a resolution of 25.39 line pairs per mm.

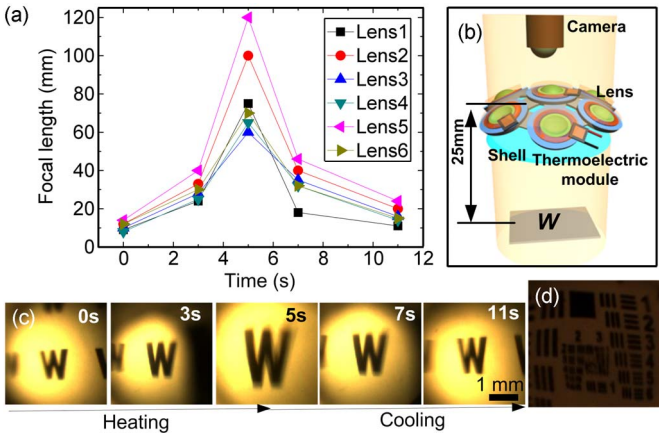

Fig. 4. Dynamic change in the back focal length of each microlens, as labeled in Fig. 1(c), in one scanning cycle. (b) Three-dimensional schematic of the setup for testing the imaging capability of the microlens array. (c) Frame sequence of the focused images from one typical microlens (number 2) in this microlens array in one scanning cycle. Thermoelectric module is converted from a heater to a cooler at 5 s. The real images are magnified before 5 s. Then, the image shrinks until 11 s. The scale bar is 1 mm. (d) Image of USAF 1951 resolution test chart obtained by one liquid microlens. The object distance is 36 mm with a focal length of 10 mm. The smallest feature is 25.39 line pairs per mm, which corresponds to Group 4, Element 5 in the chart.

V. Simulation of Thermal Behavior

Finite-element method (ANSYS; ANSYS, Inc., Canonsburg, PA) was employed to quantitatively analyze the thermal behavior of the GO-GMA-hydrogel microlens array involving the thermoelectric modules. A model of the six-element microlens array structure, including the PDMS substrates and bridges, was first established in ANSYS. The parameters set for this model were as follows: PDMS structural material; mass density: 0.97 kg/m^3; Young's modulus: 750 kPa; Poisson ratio: 0.49; thermal conductivity: 0.15 W/m · K; specific heat: 1.46 kJ/kg · K; thermal expansion ratio of 331 ppm; average convection heat transfer coefficient: 10 W · m^{-2} [21], [22]; environment temperature and initial temperature condition: 23 °C; diameter and thickness of one complete circular polymer structure representing the fringe and the substrate of a microlens: 3 and 0.5 mm, respectively; diameter and thickness of a chamber where the microlens (water-oil interface) resides: 1.5 and 0.25 mm, respectively; and connection bridge structures: 1.5 mm × 1.2 mm × 0.25 mm.

A. Heat Delivery and Conduction

With the thermoelectric modules, local thermal delivery and conduction are significantly enhanced during the actuation procedure of the microlens array. As a result, the response time of the lenses is improved. ANSYS was employed to quantitatively analyze the heat conduction in the structure involving the thermoelectric modules. A model of the six-element microlens array structure, including the PDMS substrates and bridges, with individual thermoelectric module was established in ANSYS. Thermal transient analysis was then performed. Tuning from short focal length to long focal length (forward cycle) and that from long focal length to short focal length (reverse cycle) were simulated separately, as shown in Fig. 5. Thermal boundary condition was applied at the outer area of each lens to mimic the functionality of the thermoelectric modules [refer to Fig. 1(f) for their positions]. The temperature provided by the thermoelectric modules was set as 65 °C in the forward cycle and 15 °C in the reverse cycle at the bottom of the polymer substrate. In the forward cycle, the beginning temperature of the whole structure was set at 23 °C (room temperature), while in the reverse cycle, it was set at 55 °C. Steady temperature profiles of the microlens array in the forward and reverse cycles are shown in Fig. 5(a) and (c), respectively. A point far from the thermoelectric module in the inner circular wall where the hydrogel actuator resided was monitored, as shown in Fig. 5(b) (forward cycle) and 5(d) (reverse cycle). In the forward cycle, the point is heated to 39 °C within 0.4 s. Similarly, in the reverse cycle, the temperature at this point decreases below 23 °C within 0.2 s. The simulation results confirm that thermoelectric module could rapidly increase or decrease the temperature near the hydrogel actuators.

B. Thermal Stress

Since the actuation of the GO-GMA-hydrogel-driven microlens array requires thermal variance, thermal stress, which could deform the polymer structure, might potentially degrade the optical performance of the liquid microlenses. Quantitative simulation of thermal stress based on current microlens structure was thus studied in ANSYS as well. As the highest temperature reached in the actuation process by the thermoelectric modules, 65 °C was set as the boundary condition in the model. Only the origin area of this model was fixed as a mechanical boundary condition in the simulation, which gives enough freedom for the polymer structure to deform under thermal stress. Simulated displacement of and thermal stress distribution in the planar six-element microlens array are plotted in Fig. 6(a) and (b), respectively. Most introduced stress is less than 500 Pa, and displacement is relatively small, which generally should not affect the optical performance of the microlens array in the current design. Displacement of and thermal stress distribution in the planar six-element microlens array in wrapping state are shown in Fig. 6(c) and (d), respectively. Fifty millimeters of displacement is applied at the center point of the middle lens. The edge points of the other five periphery lenses are fixed in order to mimic the wrapping behavior. Compared with the displacement and the stress induced by wrapping, the thermal stress induced into the microlens structure could be neglected. Even at the central area where we limited the degree of freedom, wrapped structure bears a stress more than 20 times of that of thermal stress (425 versus 20 kPa). Also noteworthy is that, in Fig. 6(d), the stress induced owing to the wrapping mostly appears in the thinner connection bridge structures. This is consistent with our previous report [8] and confirms that the lens structures are relatively intact after the wrapping of the complete device onto a curvilinear surface.

C. Thermal Crosstalk Between Adjacent Microlenses

Each microlens in the six-element microlens array can be individually tuned by its own hydrogel actuator. However,

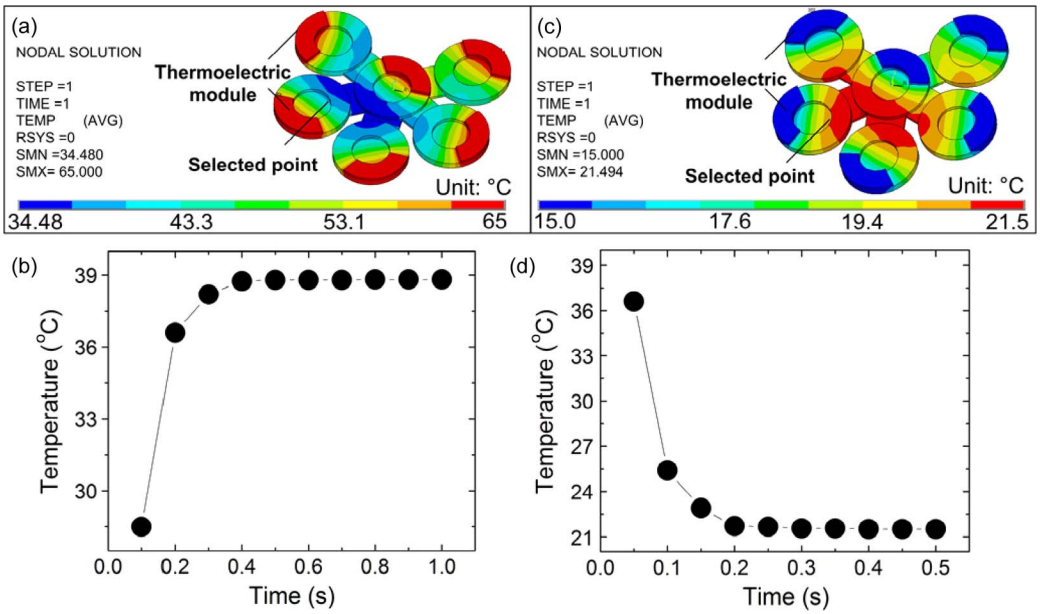

Fig. 5. (a) Temperature profile obtained from transient analysis in ANSYS of the six-element microlens array during the forward cycle. (b) Dynamic temperature change at a point of the hydrogel actuator in the forward cycle. (c) Temperature profile from the transient analysis of the same array during the reverse cycle. (d) Dynamic temperature change at the same point of the hydrogel actuator in the reverse cycle.

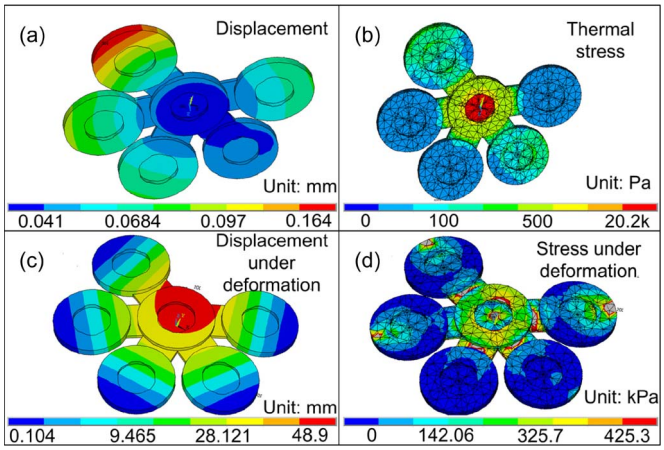

Fig. 6. (a) and (b) Displacement and thermal stress profile obtained from static analysis of a six-element microlens array in ANSYS. (c) and (d) Displacement of and thermal stress distribution in the planar six-element microlens array under small wrapping force.

the thermal variance that causes one actuator to expand or shrink might affect neighboring hydrogel actuators due to heat transfer. Hence, crosstalk between each microlens may affect the tuning process when adjacent microlenses are meant to be tuned at different focal lengths. ANSYS was then used to analyze thermal crosstalk in the six-element microlens array. In this simulation, 65 °C was considered the highest temperature needed to realize the state with the longest focal length of the GO-GMA-hydrogel-based microlens array, while 15 °C was taken as the lowest temperature boundary loaded to reach the shortest focal length. Three situations regarding the thermal crosstalk were simulated to exhibit the effect of crosstalk.

The first situation is when the central part is cooled down with a 15-°C thermal boundary to reach the shortest focal length, while adjacent microlenses are heated with a 65-°C thermal boundary to achieve the longest focal length. This would be one worst case scenario with the most severe thermal crosstalk, in which the central microlens might suffer from shifting from its shortest-focal-length state, owing to thermal crosstalk from adjacent structures. Obtained from transient and static finite-element simulations, the thermal profile of the six-element microlens array in this scenario is shown in Fig. 7(a). The temperature surrounding the GO-GMA hydrogel at the central lens is well below 32 °C, the lowest critical solution temperature (LCST) of the PNIPAAm hydrogel [15], [16], while the temperature surrounding the GO-GMA hydrogel at adjacent microlenses is well above 32 °C, as shown in Fig. 7(a). This indicates that the hydrogel actuator at the central lens would not experience any significant shrinkage, thus keeping the lens at its shortest-focal-length state. In contrast, other hydrogel actuators would still be close to their most contracted state, maintaining the longest focal length for their corresponding lenses.

Another situation is simulated as shown in Fig. 7(b). The central microlens is heated with a 65-°C boundary condition to trigger the longest-focal-length state while the adjacent microlenses are cooled down with a 15-°C boundary condition to achieve the shortest focal length. This would be another worst case scenario where the most severe thermal crosstalk would occur, since the central microlens might potentially be driven off from its longest-focal-length state by the adjacent cooler temperature. Simulation results from the transient and static finite-element analyses are plotted in Fig. 7(b). As can be seen in the temperature profile, the temperature surrounding the GO-GMA hydrogel at the central lens is well above 32 °C, the LCST of PNIAAm hydrogel, while the temperature at the adjacent lenses is much lower than 32 °C. Similar to the discussion pertaining to the first scenario, the central lens would

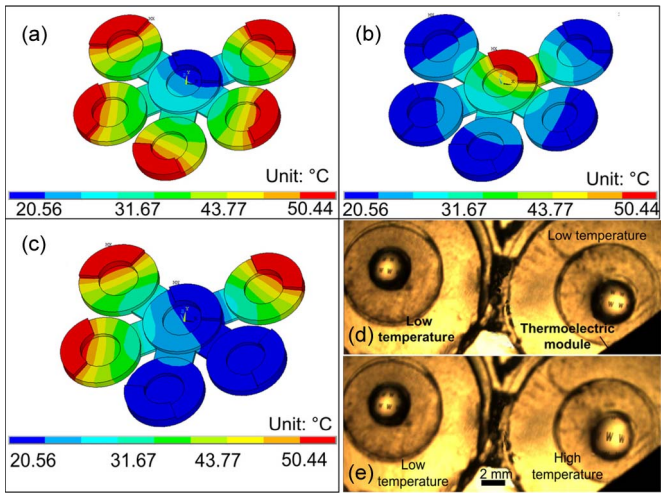

Fig. 7. Study of the thermal crosstalk between the lenses. (a) Temperature profile of the first scenario. The microlens at the center is with a 15-°C thermal boundary to activate the shortest focal length, and adjacent microlenses are with a 65-°C thermal boundary to achieve the longest focal length. The hydrogel region of the central lens is with a temperature below 15 °C, which is much lower than the LCST of the hydrogel, which ensures the short focal length. (b) Temperature profile of the second situation. The microlens at the center is with a 65-°C thermal boundary condition, and adjacent microlenses are with a 15-°C thermal boundary. The hydrogel region of the central lens is with a temperature above 35 °C, which ensures a long focal length. (c) Temperature profile of the third scenario. The central microlens is with a 15-°C thermal boundary, and the three adjacent microlenses are with a 65-°C thermal boundary. (d) Focused image of two adjacent microlenses at room temperature. Both lenses are at their short-focal-length state. (e) Focused image of two adjacent microlenses when the thermoelectric module is activated as a heater for 5 s. The right microlens reaches its long-focal-length state. The left microlens still remains at the short-focal-length state.

still have a focal length close to the longest, while the adjacent ones would have focal lengths close to the shortest. The ratio of the temperature change at the central microlens induced by crosstalk is around 15% in both of these two worst case scenarios.

The third situation simulated is when the central microlens is cooled down with a 15-°C boundary condition to realize the shortest focal length, while three adjacent microlenses are heated up to 65 °C for the longest focal length. The simulated temperature profile resulting from the transient and static finite-element analyses is shown in Fig. 7(c). The central microlens and the two adjacent microlenses without any thermal boundary condition have a temperature much lower than LCST. The other three adjacent microlenses with high-temperature boundary condition have a temperature well above the LCST.

Experiments were further performed to confirm the results from simulation. As shown in Fig. 7(d), two adjacent microlenses were at their short-focal-length state at room temperature. The right microlens was connected with a thermoelectric module. When the thermoelectric module functioned as a heater, the right microlens was transformed to a large-focal-length state, as shown in Fig. 7(e). The left microlens kept its short-focal-length state during the process.

In summary, we conclude from the simulation and experimental results that the microlenses in the six-element array under the current design would function without much disturbance by thermal crosstalk between adjacent microlenses.

D. *Effect of Positioning of Thermoelectric Modules*

Aside from simulating scenarios with thermoelectric modules on the side of the aperture, we also performed simulation with thermoelectric modules positioned directly at the bottom of the liquid microlens onto the back of the PDMS substrate.

First, we performed transient analysis similar to that in Fig. 5. The bottom surfaces of each microlens are applied with thermal boundary conditions to mimic the functionality of the thermoelectric modules. As in the simulation related to Fig. 5, in the forward cycle, the beginning temperature of the whole structure was set to be 23 °C, and at zero time instant, the temperature at all the bottom areas of the lenses became 65 °C (i.e., thermoelectric module on as heater). Similarly, in the reverse cycle, the initial temperature of the structure was 55 °C, and the bottom area of each lens became 15 °C (i.e., thermoelectric module on as cooler). Also similar to Fig. 5(b) and (d), a point at the far end of the hydrogel actuator was chosen to monitor its transient temperature both in the forward and reverse cycles, respectively. Fig. 8(a) shows the temperature profile of the steady state, and Fig. 8(b) shows the transient response time of the chosen point in the forward cycle. Fig. 8(c) and (d) shows the result for the reverse cycle. As can be seen, the results are quite comparable with those shown in Fig. 5.

We further studied three scenarios related to the crosstalk when the thermoelectric modules are placed directly below the lenses, rather than at the outer area. Again, the highest temperature was set at 65 °C, and the lowest temperature was set at 15 °C. The results are shown in Fig. 9. Fig. 9(a) shows the steady state of the first scenario, where the bottom of the central lens was at 15 °C and the bottom of the other lenses was at 65 °C. Fig. 9(b) shows the steady state of the second scenario opposite to the first one, where the bottom of the central lens was at 65 °C and the others at 15 °C. Fig. 9(c) corresponds to the third scenario where the bottom of the central lens was set at 15 °C, three others at 65 °C, and the last two without thermoelectric modules. The results in Fig. 9 are comparable to those in Fig. 7, and similar discussion would apply; hence, similar conclusion can be drawn that the thermal crosstalk is not significant.

From the simulation shown in Figs. 8 and 9, we can conclude that, in terms of tuning speed and crosstalk, the positioning of the thermoelectric modules does not make much difference in lens actuation. This would add flexibility to the system design dependent on the application and other restraints.

VI. IR Light Actuation

With large IR light absorption from GO within the hydrogel networks and superior photothermal conversion [15], [19], [22], the GO-GMA-hydrogel-based microlens array could also respond to IR light.

The optical characterization of the IR response of the microlens array is shown in Fig. 10. Initially, the microlens array was set at the shortest focal length (0 s). Then, IR light was turned on to contract the hydrogel for 10 s (forward cycle). Subsequently (at 10 s), IR was turned off (reverse cycle). The

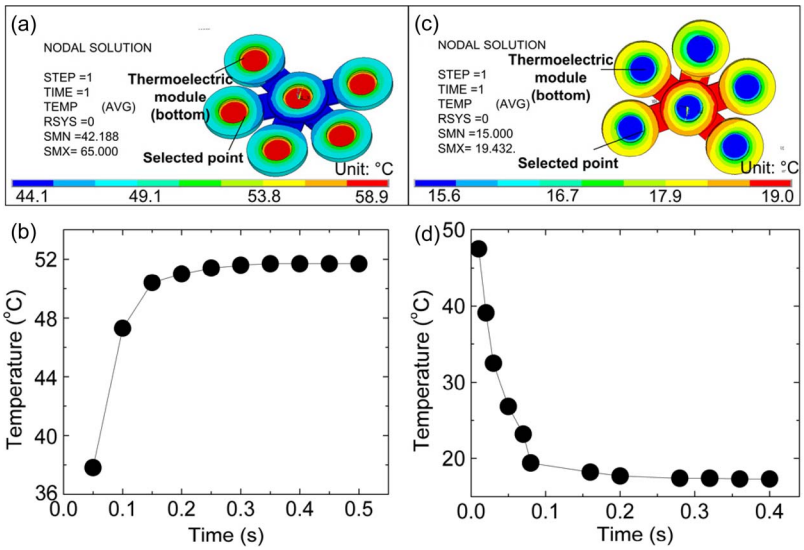

Fig. 8 Transient simulation results with thermal boundaries set at the bottom of each microlens. (a) Temperature profile obtained from the transient analysis of the six-element microlens array with thermoelectric modules at the bottom during the forward cycle. (b) Dynamic temperature change at a point of the hydrogel actuator in the forward cycle. (c) Temperature profile from the transient analysis of the same array during the reverse cycle. (d) Dynamic temperature change at the same point of the hydrogel actuator in the reverse cycle.

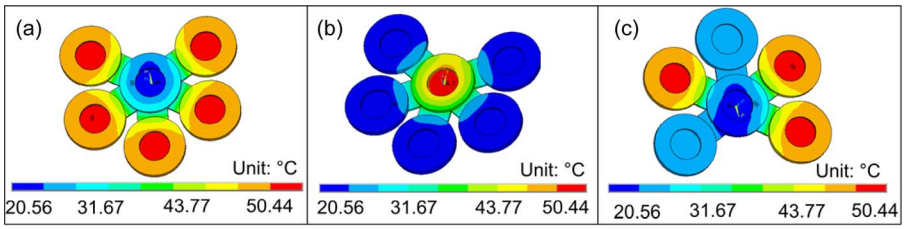

Fig. 9 Thermal crosstalk simulation with thermal boundaries set at the bottom of each microlens. (a) Temperature profile of the first scenario with a 15-°C thermal boundary at the central microlens and a 65-°C thermal boundary at adjacent microlenses. The temperature at the hydrogel region of the central lens is much lower than the LCST of the hydrogel. (b) Temperature profile of the second situation with a 65-°C thermal boundary at the central microlens and a 15-°C thermal boundary at adjacent microlenses. The temperature at the hydrogel region of the central lens is much higher than the LCST. (c) Temperature profile of the third scenario. The central microlens is with a 15-°C thermal boundary, and the three adjacent microlenses are with a 65-°C thermal boundary.

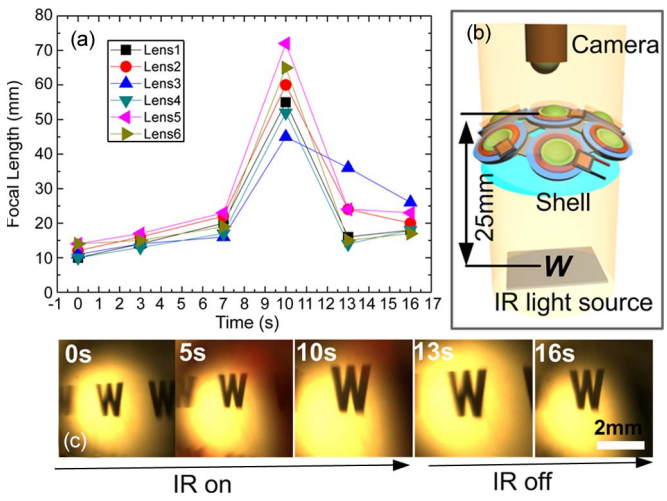

Fig. 10. (a) Dynamic change in the focal length of each microlens driven by IR, as labeled in Fig. 1(c), in one scanning cycle. (b) Three-dimensional schematic of the setup for testing the imaging capability of the microlens array. (c) Frame sequence of the focused images from one typical microlens (number 4) in the microlens array in one scanning cycle. IR is turned on at 0 s and turned off at 10 s. The real images are magnified before 10 s. Then, the image shrinks until 16 s. The scale bar is 2 mm.

focal length of the microlens gradually decreased until 16 s. Note that the thermoelectric module operates as a cooler to compensate for the temperature variance induced in the forward cycle, resulting in faster response time.

The dynamic change in the focal length of each microlens in the array in one scanning cycle driven by IR is plotted in Fig. 10(a). Focal length was recorded at 0, 3, 7, 10, 13, and 16 s, respectively, in one testing cycle. They varied from several millimeters to more than 70 mm. At 10 s, the focal lengths of all microlenses reached their maximum values.

The setup to test the imaging of the GO-GMA-hydrogel microlens array on the shell but driven by IR is shown in Fig. 10(b), which is similar to the one used for thermal tuning procedure [Fig. 4(b)]. The size of the object letter "W" was 4 mm. The frame sequence from the recorded video of one typical microlens (number 4) in one scanning cycle is shown in Fig. 10(c). The images were magnified before 10 s when IR was turned on (intensity: 28 mW/cm^2), indicating an increase in focal length; the image scaled back after 11 s when IR was turned off, indicating a decrease in focal length. During the whole recording process, the stereoscope was fine-tuned to keep the images clear.

VII. Conclusion

In summary, we have demonstrated a liquid-based GO-GMA-hydrogel-driven microlens array on a curvilinear surface that processes large-focal-length tuning range, large FOV, and relatively fast response time. Thermoelectric modules based on Peltier effect were applied to improve the heat delivery to and dissipation from the hydrogel actuators. The focal length ranged from several millimeters to over 100 mm, and the response time improved to 5 s. Finite-element simulation was performed to study the thermal response during the actuation. Good thermal performance of the microlens array was demonstrated by simulation and experiments regarding thermal stress and crosstalk between adjacent microlenses during the actuation procedure. In addition, it was also shown that the microlens array could be controlled remotely via IR irradiation. Characterization of the IR response of the microlens array was performed. The focal length ranged from several millimeters to 70 mm, and the average response time was 8 s.

In the future, optical quality of the microlens array such as achromatic aberration caused by light passing through different layers of materials (PDMS, water, and oil) with different refractive indices would be further studied. The liquid lens interface profile can be further investigated [24] for more comprehensive optical characterization. An IR thermal camera would be used to monitor the actuation procedure for quantitative analysis. Uniformity of the microlenses will be improved by using better lithography systems and precise pipetting to control the volume of the water filled into the cavities. Reliability of the microlenses in terms of number of actuation cycles and shelf-time as well as packaging method to avoid liquid leakage will be investigated. Microthermoelectric devices will be fabricated and integrated with the microlenses. Material properties of GO-GMA hydrogel will be further studied for theoretical focal length calculation. Quantitative structural analysis on actuation mechanism will be performed to better characterize the lens tuning process. Multiple waveguides could be employed to simultaneously transmit the signal obtained from different microlenses [25]. Further research on IR would be conducted, since this approach paves a way to intrinsically integrate such tunable microlenses with other optical components, such as optical fibers and switches [13].

Acknowledgment

The authors would like to thank Dr. X. Zeng for the technical discussions and Computer Aided Engineering, University of Wisconsin, Madison, for the access to ANSYS 12.1.

References

[1] D. Zhang, V. Lien, Y. Berdichevsky, J. Choi, and Y.-H. Lo, "Fluidic adaptive lens with high focal length tunability," *Appl. Phys. Lett.*, vol. 82, no. 19, pp. 3171–3172, May 2003.

[2] K. Carlson, M. Chidley, K. B. Sung, M. Descour, A. Gillenwater, M. Follen, and R. Richards-Kortum, "*In vivo* fiber-optic confocal reflectance microscope with an injection-molded plastic miniature objective lens," *Appl. Opt.*, vol. 44, no. 10, pp. 1792–1797, Apr. 2005.

[3] H. Ren and S. T. Wu, "Variable-focus liquid lens by changing aperture," *Appl. Phys. Lett.*, vol. 86, no. 21, pp. 211107-1–211107-3, May 2005.

[4] C.-C. Cheng, C. A. Chang, C.-H. Liu, and J. A. Yeh, "A tunable liquid-crystal microlens with hybrid alignment," *J. Opt. A, Pure Appl. Opt.*, vol. 8, no. 7, pp. 365–369, Jul. 2006.

[5] A. Jain and H. Xie, "Microendoscopic confocal imaging probe based on an LVD microlens scanner," *IEEE J. Sel. Top. Quantum Electron.*, vol. 13, no. 2, pp. 228–234, Mar./Apr. 2007.

[6] T. Krupenkin, S. Yang, and P. Mach, "Tunable liquid microlens," *Appl. Phys. Lett.*, vol. 82, no. 3, pp. 316–318, Jan. 2003.

[7] D. Zhu, C. Li, X. Zeng, and H. Jiang, "Tunable-focus microlens arrays on curved surfaces," *Appl. Phys. Lett.*, vol. 96, no. 8, p. 081 111, Feb. 2010.

[8] D. Zhu, X. Zeng, C. Li, and H. Jiang, "Focus-tunable microlens arrays fabricated on spherical surfaces," *J. Microelectromech. Syst.*, vol. 20, no. 2, pp. 389–395, Apr. 2011.

[9] S. Grilli, L. Miccio, V. Vespini, A. Finizio, S. De Nicola, and P. Ferraro, "Liquid micro-lens array activated by selective electrowetting on lithium niobate substrates," *Opt. Exp.*, vol. 16, no. 11, pp. 8084–8093, May 2008.

[10] J. Chen, W. S. Wang, J. Fang, and K. Varahramyan, "Variable-focusing microlens with microfluidic chip," *J. Micromech. Microeng.*, vol. 14, no. 5, pp. 675–680, May 2004.

[11] C. A. Lopez, C. C. Lee, and A. H. Hirsa, "Electrochemically activated adaptive liquid lens," *Appl. Phys. Lett.*, vol. 87, no. 13, pp. 134102-1–134102-3, Sep. 2005.

[12] L. Dong, A. K. Agarwal, D. J. Beebe, and H. Jiang, "Adaptive liquid microlenses activated by stimuli-responsive hydrogels," *Nature*, vol. 442, pp. 551–554, Aug. 2006.

[13] X. Zeng and H. Jiang, "Tunable liquid microlens actuated by infrared light-responsive hydrogel," *Appl. Phys. Lett.*, vol. 93, no. 15, p. 151 101, Oct. 2008.

[14] Z. Ding and B. Ziaie, "A pH-tunable hydrogel microlens array with temperature-actuated light-switching capability," *Appl. Phys. Lett.*, vol. 94, no. 8, p. 081 111, Feb. 2009.

[15] C.-W. Lo, D. Zhu, and H. Jiang, "An infrared-light responsive graphene-oxide incorporated poly(*N*-isopropylacrylamide) hydrogel nanocomposite," *Soft Matter*, vol. 7, no. 12, pp. 5604–5609, 2011.

[16] C.-W. Lo, D. Zhu, and H. Jiang, "Microfluidic actuators based on infrared-light responsive PNIPAAm hydrogel nanocomposite incorporating graphene-oxide," in *Proc. 16th Int. TRANSDUCERS*, Beijing, China, 2011, pp. 2430–2433.

[17] Y. N. Xia and G. M. Whitesides, "Soft lithography," *Annu. Rev. Mater. Sci.*, vol. 28, pp. 153–184, 1998.

[18] A. A. Balandin, S. Ghosh, W. Bao, I. Calizo, D. Teweldebrhan, F. Miao, and C. N. Lau, "Superior thermal conductivity of graphene," *Nano Lett.*, vol. 8, pp. 902–907, 2008.

[19] K. Haubert, T. Drier, and D. Beebe, "PDMS bonding by means of a portable, low-cost corona system," *Lab Chip*, vol. 6, no. 12, pp. 1548–1549, 2006.

[20] X. Zeng, C. Li, D. Zhu, H. Cho, and H. Jiang, "Tunable microlens arrays actuated by various thermo-responsive hydrogel structures," *J. Micromech. Microeng.*, vol. 20, no. 11, p. 115 035, Nov. 2010.

[21] C.-H. Cho, W. Cho, and A. S.-Y. Hwang, "PDMS-glass serpentine microchannel chip for time domain PCR with bubble suppression in sample injection," *J. Micromech. Microeng.*, vol. 17, no. 9, pp. 1810–1817, Sep. 2007.

[22] *Material Property Database*, Feb. 2004, [Online]. Available: http://www.mit.edu/~6.777/matprops/pdms.htm

[23] V. Abdelsayed, S. Moussa, H. M. Hassan, H. S. Aluri, M. M. Collinson, and M. S. El-Shall, "Photothermal deoxygenation of graphite oxide with laser excitation in solution and graphene-aided increase in water temperature," *J. Phys. Chem. Lett.*, vol. 1, no. 19, pp. 2804–2809, 2010.

[24] C. Li, G. Hall, X. Zeng, D. Zhu, K. Eliceiri, and H. Jiang, "Three-dimensional surface profiling and optical characterization of liquid microlens using a Shack–Hartmann wavefront sensor," *Appl. Phys. Lett.*, vol. 98, no. 17, p. 171 104, Apr. 2011.

[25] K.-H. Jeong, J. Kim, and L. P. Lee, "Biomimetic artificial compound eyes," *Science*, vol. 312, pp. 557–561, 2006.

Difeng Zhu received the B.S. degree in microelectronics from Peking University, Beijing, China, in 2007, and the Ph.D. degree in electrical engineering from the University of Wisconsin, Madison, in 2011.

He is currently an R&D Process Engineer with Micron Technology Inc., Boise, ID. His research interests include liquid microlens array, microelectronics, and microelectromechanical systems fabrication process.

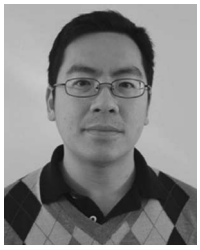

Chi-Wei Lo received the B.S. degree in chemistry from the National Tsing Hua University, Hsinchu, Taiwan, in 2001, the M.S. degree in materials science from the University of Pennsylvania, Philadelphia, in 2006, and the Ph.D. degree in materials science program from the University of Wisconsin, Madison, in 2011.

He is currently an R&D Process Engineer with Applied Materials, Inc., Santa Clara, CA. His research interests include graphene-oxide-incorporated hydrogel nanocomposites, microfluidics, and solar energy harvesting devices.

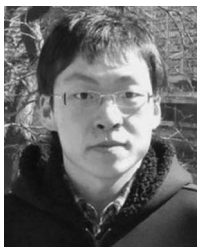

Chenhui Li received the B.S. degree in electrical engineering from Tsinghua University, Beijing, China, in 2007, and the M.S. degree in electrical and computer engineering from the University of Wisconsin, Madison, in 2010, where he is currently working toward the Ph.D. degree in electrical engineering.

His research interests include micro-optical imaging, liquid focus-variable microlenses, electrowetting, and light field cameras.

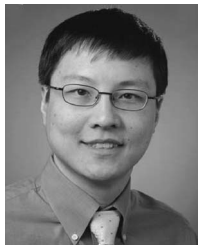

Hongrui Jiang (S'98–M'02–SM'10) received the B.S. degree in physics from Peking University, Beijing, China, and the M.S. and Ph.D. degrees in electrical engineering in 1999 and 2001, respectively, from Cornell University, Ithaca, NY.

From 2001 to 2002, he was a Postdoctoral Researcher with the Berkeley Sensor and Actuator Center, University of California at Berkeley. He is currently an Associate Professor in the Department of Electrical and Computer Engineering, a Faculty Affiliate in the Department of Biomedical Engineering, a Faculty Member of the Materials Science Program, and a Member of the Eye Research Institute, University of Wisconsin, Madison. He is a currently a member of the Editorial Board of the JOURNAL OF MICROELECTROMECHANICAL SYSTEMS. His research interests are in microfabrication technology, biological and chemical microsensors, microactuators, optical microelectromechanical systems, smart materials and micro-/nanostructures, lab on a chip, and biomimetics and bioinspiration.

Dr. Jiang was the recipient of a National Science Foundation CAREER Award and the Defense Advanced Research Projects Agency Young Faculty Award in 2008, the H. I. Romnes Faculty Fellowship of the University of Wisconsin in 2011, and the NIH Director's New Innovator Award in 2011.